STEREOSCOPIC PIV MEASUREMENTS IN A JET IN CROSSFLOW

Knud Erik Meyer, Oktay Özcan*, Poul S. Larsen
Department of Mechanical Engineering,
Technical University of Denmark
DK-2800 Kgs. Lyngby, Denmark
kem@mek.dtu.dk

Carsten H. Westergaard
Dantec Measurement Technology A/S
Tonsbakken 16-18, DK-2740 Skovlunde, Denmark

ABSTRACT

Stereoscopic Particle Image Velocimetry (PIV) has been used to measure all components of the velocity vector and the Reynolds stress tensor in several planes for a jet in crossflow. The Reynolds number based on the free stream velocity and the jet diameter was 2400. Jet-to-crossflow velocity ratios of 1.3 and 3.3 were investigated. The general structure of the flow and turbulence is discussed. Data obtained in two closely spaced parallel planes were used to calculated the rate-of-deformation tensor. This is used to demonstrate the extent of failure of the Boussinesq approximation for complex flow.

INTRODUCTION

Jets in a crossflow are of great practical relevance in a variety of engineering applications such as V/STOL aircraft, chemical unit operations, gas turbines and waste disposal into water bodies or the atmosphere. The characteristics of a jet in crossflow are primarily dependent on the ratio of the jet to crossflow momentum R (or the velocity in case of unheated and incompressible flows). As reported by Andreopoulos and Rodi (1984), at high velocity ratios R the near field of jets in a crossflow is controlled largely by complex inviscid dynamics and the flow further downstream is influenced by turbulence. In contrast, even the near field is dominated by turbulence for small velocity ratios. Experiments by Fric and Roshko (1994) and Kelso et. al. (1996) show that there exists a complex vortical flow structure in the near field of a jet in a crossflow. In addition to the horse-shoe vortex, ring-like vortices (jet shear–layer vortices) and counter rotating bound vortex pair, Fric and Roshko (1994) observed up-right wake vortices which extend vertically from the wall to the jet.

There is a scarcity of turbulence data for the near flow field of a transverse jet. The majority of existing experimental data were obtained with hot-wire anemometry which is insensitive to flow direction and can give large errors in regions of high turbulent kinetic energy which may here be larger than the mean kinetic energy of the cross flow. However, data presented by Larsen et. al. (1994), Crabb et. al. (1981) and Özcan and Larsen (2001) give good insight into physical structure of a jet in crossflow. More recently velocity fields have been studied by PIV (Kim et. al., 1999). Meyer et. al. (2000) and Özcan et. al. (2001) present PIV/PLIF data for a water jet issuing into a fully-developed flow in a water channel.

The present paper reports stereoscopic PIV measurements carried out in a wind tunnel near the exit of a jet in crossflow. The data include three components of the mean velocity and six components of the Reynolds stress tensor for jet-to-crossflow velocity ratios of $R = 3.3$ and $R = 1.3$. Measurements were performed at several planes. Data obtained in two closely spaced parallel planes were used to calculate all components of the rate-of-deformation tensor. Results are discussed in terms of topologies of sectional streamlines, turbulent shear stress vector and shear deformation vector.

EXPERIMENTAL SET-UP

Experiments were conducted in a wind tunnel with test section width equal to 300 mm and height equal to 600 mm. The Reynolds

*On leave from Dept. of Aero. and Astro., Tech. University of Istanbul

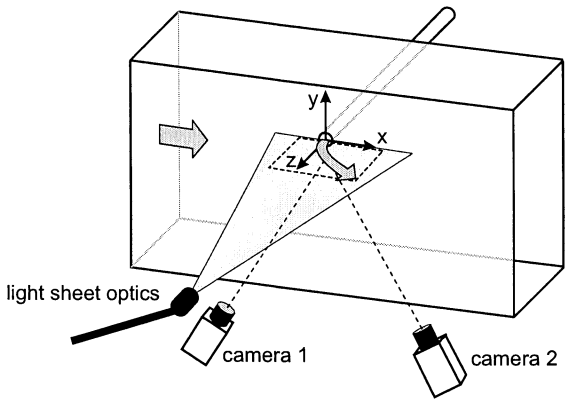

Figure 1: Experimental set-up. Cameras and light sheet optics are mounted on the same traversing unit.

number based on the free stream velocity (U_∞ = 1.5 m/s) and the jet diameter (D = 24 mm) was nominally 2400. The jet issued normal to a flat plate raised from the side wall of the tunnel. The length of the pipe employed to produce the jet flow was sufficiently large so that fully developed pipe flow approached the jet exit. The boundary layer on the flat plate approaching the jet was also turbulent with a boundary layer thickness of $\delta_{99\%} \simeq 70$ mm. More details of the experimental set-up are described in Özcan and Larsen (2001) which reports LDA measurements in the incoming pipe flow and flat plate boundary layer. These measurements show that characteristics of turbulence in incoming flows agree well with experimental and computational data available in the literature. It was important to establish and document well-defined incoming conditions of this flow because computational studies have been known to be fairly sensitive to the state of turbulence in incomings flows (see Yuan et. al., 1999).

Measurements of components of mean velocity and Reynolds stress were carried out by using a digital stereoscopic PIV system as illustrated in figure 1. The system consisted of two Kodak Megaplus ES 1.0 cameras with 60 mm Nikon lenses mounted in Scheimpflug condition. The angle between the cameras was approximately 80° and the recordings used an F-number of 2.8. The light sheet was created with a double cavity Nd-YAG laser delivering 100 mJ light pulses. A light guiding arm was used to connect the laser with the light sheet forming optics. Both the light sheet forming optics and the cameras were mounted on the same traversing unit. The light sheet thickness was 1.5 mm.

Seeding consisting of 2-3 μm droplets of glycerine was added to both the main flow and the jet. The seeding density in main flow and jet was adjusted to be equal based on visual evaluation of the PIV images. The measuring system was controlled by a Dantec PIV2100 processor and the data was processed with Dantec Flowmanager version 3.4 using adaptive velocity correlation. A 25% overlap was used between interrogation areas. The geometrical information needed for the reconstruction of the three components of velocity was based on images of a calibration target. Images of the target (aligned with the light sheet) were taken with both cameras in five different planes in the out-of-plane direction. The reconstruction was performed by a linear transformation using the calibration. The final vectors map typically contained 33 by 36 three-component velocity vectors.

Image maps were recorded with an acqusition rate of about 0.5 Hz. 1000 instantaneous vector maps were used to calculate the processed data. Two configurations of the cameras and light sheet were used. The first configuration had the light sheet perpendicular to the wall and parallel with the free stream as illustrated in figure 1. This gave data in y-constant planes. The second configuration had the light sheet parallel to both the side wall and the free stream. This gave data in z-constant planes. For both configurations the area covered by both cameras was approximately 100 by 80 mm.

RESULTS AND DISCUSSION

Results will be presented in terms of the time-averaged velocity vector (U, V, W) and all six components of the Reynolds stress tensor $\overline{uu}$, $\overline{vv}$, $\overline{ww}$, $\overline{uv}$, $\overline{uw}$, $\overline{vw}$.

Figure 2 shows the flow in the plane of symmetry ($y = 0$) for velocity ratios of R = 1.3 and R = 3.3. Mean velocities in this plane are shown both as vectors and streamlines. Streamlines are irregularly spaced because they are started from points in a grid. The streamlines started close to the jet are all drawn into the jet. This gives an indication of the jet trajectory. A streamline started at the center of the jet is therefore used to find the jet trajectory indicated with the symbol ◇ in all plots. Yuan and Street (1998) report that among various methods used for defining the jet trajectory, the streamline trajectory is the best indicator. For R = 1.3 the jet bends into the main flow direction within 1–2 jet diameters. For R = 3.3 the jet penetrates several diameters into the main flow before a

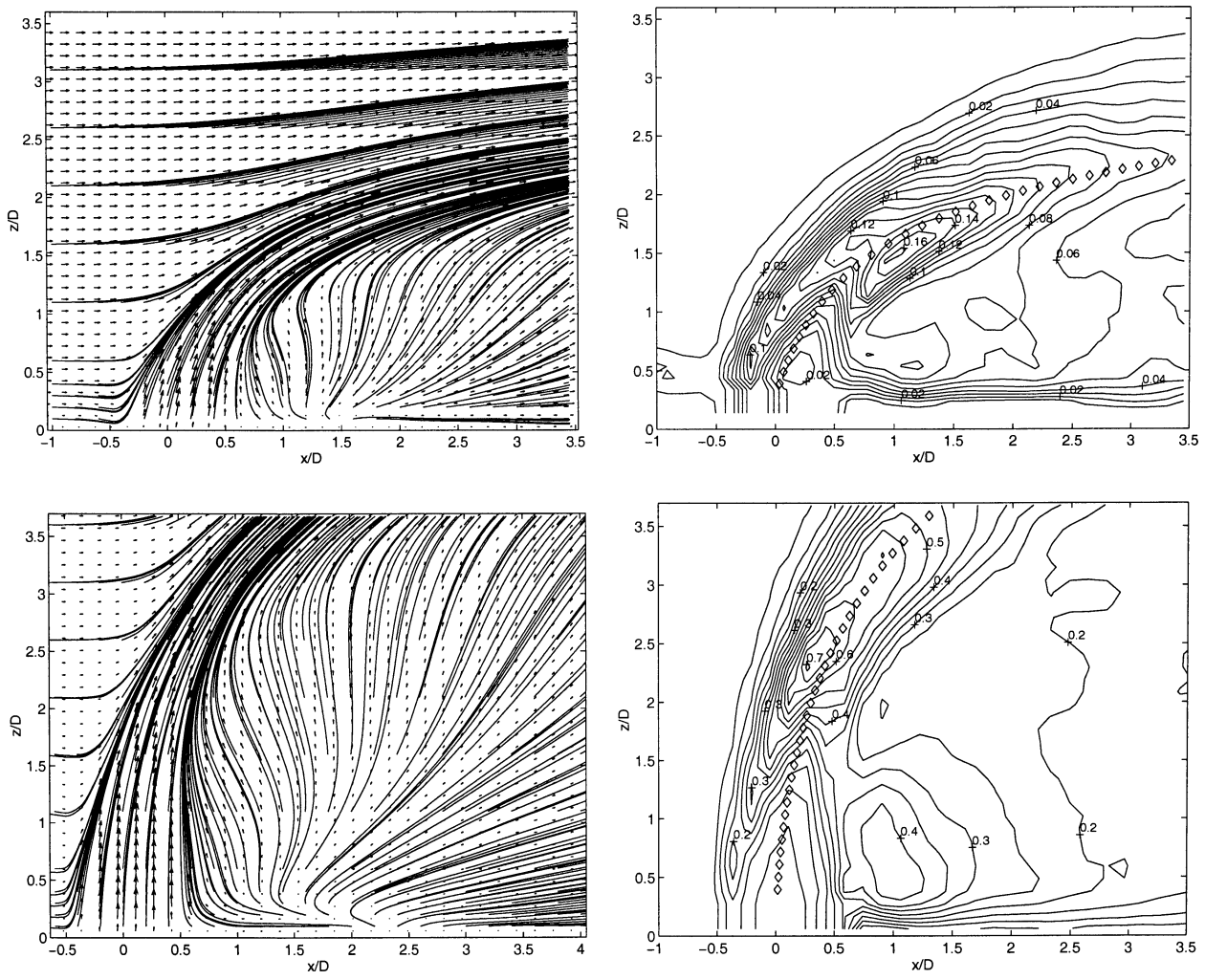

Figure 2: Data in the plane of symmetry ($y = 0$). Upper and lower are $R = 1.3$ and $R = 3.3$, respectively. Plots on the left show velocity vectors together with sectional streamlines. Plots on the right show contours of the turbulent kinetic energy $k/(U_\infty)^2$. The symbol $\diamond$ indicates the jet trajectory.

significant bend is noticed. For both velocity ratios, velocity vectors and streamlines show a region with negative U-velocity component behind the jet.

In figure 2, the first one or two rows of velocity vector inside the jet (closest to the jet exit) are clearly too small. Particle images found in this region on the second PIV image are upstream in the jet and therefore outside the first PIV image. This caused a strong velocity bias towards zero velocity. However, data in the remaining field are reliable and unbiased. Data for the first two rows of the measurement grid between $-0.5 < x/d < 0.5$ (16 points) are corrected by extrapolation from the third row in the rest of the figures.

The turbulent kinetic energy is calculated as $k = 0.5(\overline{uu} + \overline{vv} + \overline{ww})$ and plotted in figure 2. For $R = 1.3$, the maximum value of k is found slightly downstream (i.e. in x-direction) of the jet trajectory, while for $R = 3.3$ it is found

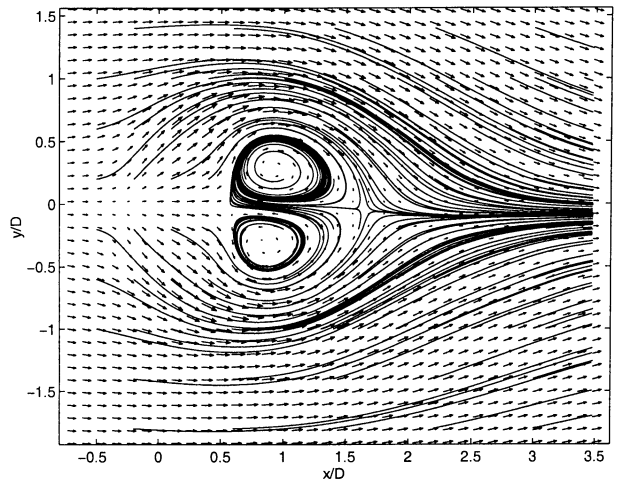

Figure 3: Velocities in the x, y-plane perpendicular to the jet, $z/D = 1.33$, $R = 3.3$. Velocity vectors are projected on the plane together with sectional streamlines.

slightly upstream of the jet trajectory. The maximum value of k is about 4.5 times greater for $R = 3.3$ than for $R = 1.3$.

Figure 3 shows mean velocities in an x, y-plane perpendicular to the jet. The sectional streamlines reveal the counter rotating vortex pair which causes a reversal of the U velocity. The vortex pair is located just downstream of the jet core indicated by merging streamlines in figure 2. The sectional streamlines indicate a slight deviation from symmetry with respect to the $y = 0$ plane. This could be caused by inaccuracies in the calibration.

Figure 4 shows the velocity vectors projected onto a y-constant plane situated one jet diameter away from the symmetry plane ($y = D$). The vectors are shown together with sectional streamlines. Velocities are larger near the jet. The out-of-plane velocity component V is positive (directed away from the jet) in the upper-left part and negative in the lower-right part. Both the magnitude of velocities and velocity gradients are much smaller than seen in figure 2. The flow has direction towards the wall just upstream of the jet and away from the wall at the jet and further downstream. A contour plot of k is also shown in figure 4. The maximum value of k is located nearly one jet diameter downstream of the jet trajectory at the $y = 0$ plane. The position of the maximum value of k coincides with a region of large velocities indicating large interaction between jet and free stream. The magnitude of the maximum value of k is almost as high as that of k found at the symmetry plane ($y = 0$).

One way to present a part of the Reynolds stress tensor is the projection of the shear stress vector of a coordinate-plane onto the plane. On a y-constant plane, this is given by the shear stress vector

$$\boldsymbol{\tau}_y = \overline{vu}\,\mathbf{i} + \overline{vw}\,\mathbf{k} \qquad (1)$$

Here, $\mathbf{i}$ and $\mathbf{k}$ are unit vectors in the x and z directions, respectively. A vector plot of $\boldsymbol{\tau}_y$ in the $y = D$ plane is shown in figure 5 (left).

The shear stress vectors can be compared to a similar vector, called shear deformation vector. This vector is based on the Boussinesq eddy viscosity model. The Boussinesq hypothesis assumes that the deviatoric Reynolds stress is proportional to, hence aligned with, the deviator of the rate-of-deformation tensor, which for incompressible flow becomes

$$-\rho\overline{u_i u_j} + \tfrac{2}{3}\rho k\delta_{ij} = \mu_t\left(\frac{\partial U_i}{\partial x_j} + \frac{\partial U_j}{\partial x_i}\right) \qquad (2)$$

where μ_t denotes the eddy viscosity. The shear deformation vector $\mathbf{D}_y$ on the y-constant plane is defined as

$$\mathbf{D}_y = \left(\frac{\partial V}{\partial x} + \frac{\partial U}{\partial y}\right)\mathbf{i} + \left(\frac{\partial V}{\partial z} + \frac{\partial W}{\partial y}\right)\mathbf{k} \qquad (3)$$

In order to calculate $\mathbf{D}_y$, gradients in the y-direction have to be evaluated. For this purpose, data have also been taken in the $y/D = 1.125$ plane.

If the Boussinesq eddy viscosity model were valid then $\boldsymbol{\tau}_y$ and $-\mathbf{D}_y$ should be aligned while the ratio of their magnitudes may vary in space. Figure 5 (right) shows a vector plot of $-\mathbf{D}_y$ for the $y = D$ plane. Comparing directions of stress and deformation vectors in figure 5 show them to not be aligned, except in some limited regions of the flow. Also, calculations of eddy viscosity μ_t from eq. (2) produces negative μ_t values in some regions of this flow. This is due to inadequacies of the Boussinesq approximation to be expected for such a complex flow. However, Özcan et. al. (2001) show that eddy viscosity could be determined with sufficient accuracy if the velocity and Reynolds stresses are transformed into a jet trajectory based coordinate system for the mid-plane.

The shear stress vector $\boldsymbol{\tau}_y$ in figure 5 has the largest magnitude in the region located slightly downstream of the jet trajectory for $z/D > 2$. Here, $\boldsymbol{\tau}_y$ is pointing upwards indicating that the shear is acting on the strong velocity gradient of W in the y direction. The region is slightly upstream of the region with the largest velocity vectors and the maximum value of k shown in figure 4. Further downstream from the jet trajectory, $\boldsymbol{\tau}_y$ is pointing upstream. This is probably due to the interaction between the low velocity region downstream of the jet in the $y = 0$ plane (see figure 2) and the free stream velocity found further away in the y-direction. Close to the jet trajectory at $z/D \approx 1.5$, $\boldsymbol{\tau}_y$ is no longer pointing upwards, but is turning towards the upstream direction. At this point the velocities shown in figure 4 are changing direction. For larger z, W is positive while for smaller z, W is negative. This is a region where the flow is changing from having large Reynolds stresses to be dominated by pressure distribution.

Overall, the shear deformation vector field $-\mathbf{D}_y$ shown in figure 5 has similarities to the the shear stress vector field. Both fields have the largest magnitudes in region slightly downstream of the jet trajectory with the direction directed upwards. However, for $z/D \leq 1.5$

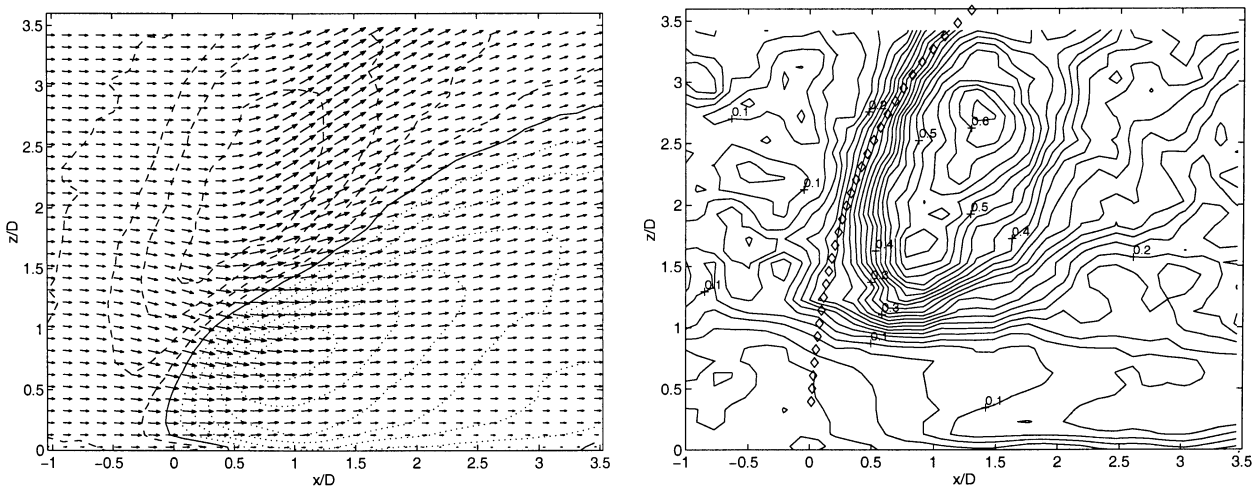

Figure 4: Data in the plane $y = D$ for $R = 3.3$. *Left:* (U, W) vectors and contours of the V velocity component (contour spacing $0.1U_\infty$, $V = 0$ solid, $V < 0$ dotted, $V > 0$ dashed). *Right:* turbulent kinetic energy $k/(U_\infty)^2$. Symbol $\diamond$ indicates jet trajectory at $y = 0$ plane.

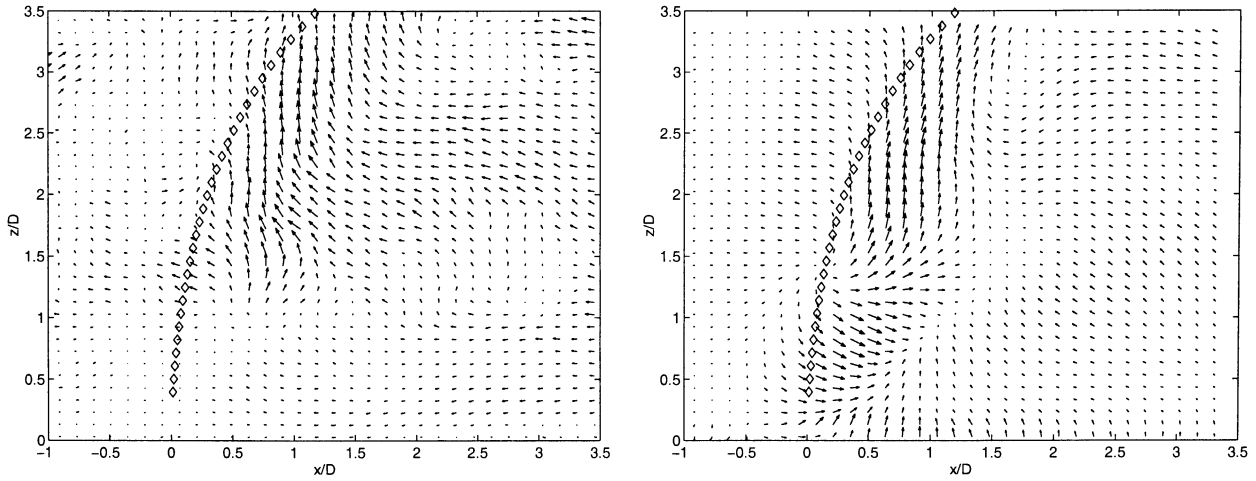

Figure 5: The shear stress vector $(\overline{vu}, \overline{vw})$ (left) and shear deformation vector $-\mathbf{D}_y$ (right) in the plane $y = D$ for $R = 3.3$. Symbol $\diamond$ indicates the jet trajectory at $y = 0$ plane.

$-\mathbf{D}_y$ has a strong component in the downstream direction. This is the opposite effect as found for $\boldsymbol{\tau}_y$. There are therefore significant deviations in the alignment of the vector fields. This indicates that numerical calculations based on Boussinesq model will have difficulties in the complex flow of a jet in cross flow.

Figure 6 shows the shear stress vector $(\overline{wu}, \overline{wv})$ in the $z/D = 1.33$ plane also shown in figure 3. The large shear stresses are found at the border of the jet core. The direction is here pointing away from the jet core acting to expand the jet. The largest values of the shear stress vector is seen at the border between the jet core and the counter rotating vortex pair shown in figure 3. The vortex pair is transporting fluid with low W velocity towards the jet core and therefore creating extra exchange

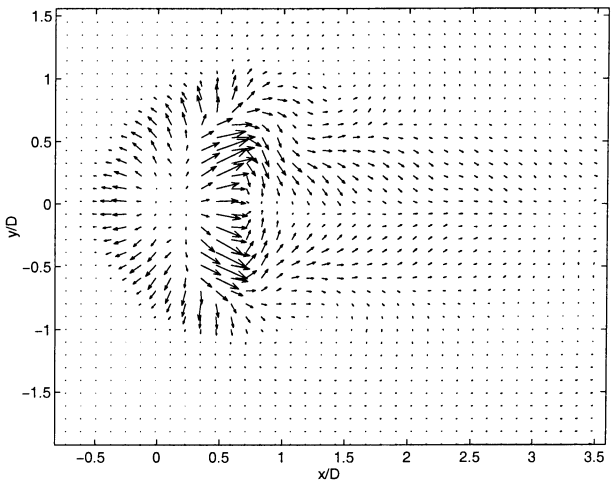

Figure 6: Shear stress vector $(\overline{wu}, \overline{wv})$ in the x, y-plane perpendicular to the jet, $z/D = 1.33$ for $R = 3.3$.

of W-momentum.

The PIV data presented in this paper generally agree well with the LDA data reported by Özcan and Larsen (2001) and the computational data by Yuan et. al. (1999). A comparison of these three data sets will be made in a separate paper. Due to differences in incoming flows, the experimental jet trajectory is slightly steeper than the computational jet trajectory of Yuan et. al. (1999).

CONCLUSION

The data presented demonstrate some of the capabilities of stereoscopic PIV. The availability of all components of mean velocity and Reynolds stress facilitates a more detailed interpretation of the complex flow features possible. As an example, turbulent kinetic energy k is calculated without the need of assumptions about missing components of the Reynolds tensor. The presented data are only a subset of a larger database covering many planes and the two velocity ratios 1.3 and 3.3. More data from this database will be presented in coming papers.

Besides giving insight into details of the complex flow of a jet in cross flow, the database can be a valuable tool for evaluation of numerical calculations using different turbulence models. The comparison of shear stress vectors and shear deformation vectors suggests the degree of failure to be expected for turbulence models based on the Boussinesq eddy viscosity model for this flow. The comparison also demonstrates that the availability of all velocity components and Reynolds stresses in a closely spaced grid makes it possible to examine other turbulence models in detail.

The combination of laser light intensity, particle size and camera does not give optimal conditions for accurate recording of particle positions. The calculated particle image size is somewhat smaller than one camera pixel. This results in some uncertainty in the estimated particle displacements. The uncertainty of estimated velocities is therefore probably 3–4 percent compared to the about one percent of the maximum velocity, that can be obtained under optimal conditions.

ACKNOWLEDGEMENTS

The second author acknowledges the financial support received from the Technical University of Denmark and the NATO Science Fellowship Program by the Scientific and Technical Research Council of Turkey.

REFERENCES

Andreopoulos, J. and Rodi, W., 1984, "Experimental investigation of jets in crossflow", *Journal of Fluid Mechanics*, Vol. 138, pp. 93-127.

Crabb, D., Durao, D.F.G. and Whitelaw, J.H., 1981, "A round jet normal to a crossflow", *Journal of Fluids Engineering*, Vol. 103, pp.142-153.

Fric, T.F. and Roshko, A., 1994, "Vortical structure in the wake of a transverse jet", *Journal of Fluid Mechanics*, Vol.279, pp.1–47.

Kelso, R.M., Lim T.T. and Perry A.E., 1996, "An experimental study of round jets in cross–flow," *Journal of Fluid Mechanics*, Vol.306, pp.111–144.

Kim, K.C., Kim, S.K. and Yoon, S.Y., 1999, "PIV measurements of the flow and turbulent characteristics of a round jet in crossflow," *Third International Workshop on Particle Image Velocimetry*, Sep.16-18, Santa Barbara, CA.

Larsen, P.S., Böhme, L. and Andresen, E., 1994, "Laser sheet tomography of jet flows," *Proceedings of the Seventh International Symposium on Applications of Laser Techniques to Fluid Mechanics*, 11-14 July, Lisbon, Portugal.

Meyer, K.E., Özcan, O., Larsen, P.S., Gjelstrup, P. and Westergaard C.H., 2000, "Point and planar LIF for velocity-concentration correlations in a jet in cross flow," *Proceedings of the Tenth International Symposium on Applications of Laser Techniques to Fluid Mechanics*, 10-13 July, Lisbon, Portugal.

Özcan,O. and Larsen, P.S., 2001, "An experimental study of a turbulent jet in crossflow by using LDA", Department Report, Department of Mechanical Engineering, Technical University of Denmark (To be published).

Özcan, O., Meyer, K.E., Larsen, P.S. and Westergaard C.H., 2001, "Simultaneous measurement of velocity and concentration in a jet in channel-crossflow," *Proceedings of the Fluids Engineering Division Summer Meeting 2001*, May 29- June 1, New Orleans, Lousiana, USA.

Yuan, L.L. and Street, R.L., 1998, "Trajectory and entrainment of a round jet in crossflow", *Physics of Fluids*, Vol. 10, pp. 2323-2335.

Yuan, L.L., Street, R.L. and Ferziger, J.H., 1999, "Large-eddy simulations of a round jet in crossflow", *Journal of Fluid Mechanics*, Vol. 279, pp. 71-104